J. Cell. Mol. Med. Vol 16, No 12, 2012 pp. 2990-3000

Characterization of the tissue-level Ca^{2+} signals in spontaneously contracting human myometrium

Gilles Bru-Mercier [a], Joanna E. Gullam [b, c], Steven Thornton [b], Andrew M. Blanks [a], Anatoly Shmygol [a, *]

[a] *Warwick Medical School, University of Warwick, Coventry, UK*
[b] *Medical School, University of Exeter, Exeter, UK*
[c] *Present address: Department of Obstetrics and Gynaecology, University of Otago, Christchurch, New Zealand*

Received: April 17, 2012; Accepted: August 28, 2012

Abstract

In the labouring uterus, millions of myocytes forming the complex geometrical structure of myometrium contract in synchrony to increase intrauterine pressure, dilate the cervix and eventually expel the foetus through the birth canal. The mechanisms underlying the precise coordination of contractions in human myometrium are not completely understood. In the present study, we have characterized the spatio-temporal properties of tissue-level $[Ca^{2+}]_i$ transients in thin slices of intact human myometrium. We found that the waveform of $[Ca^{2+}]_i$ transients and isotonic contractions recorded from thin slices was similar to the waveform of isometric contractions recorded from the larger strips in traditional organ bath experiments, suggesting that the spatio-temporal information obtained from thin slices is representative of the whole tissue. By comparing the time course of $[Ca^{2+}]_i$ transients in individual cells to that recorded from the bundles of myocytes we found that the majority of myocytes produce rapidly propagating long-lasting $[Ca^{2+}]_i$ transients accompanied by contractions. We also found a small number of cells showing desynchronized $[Ca^{2+}]_i$ oscillations that did not trigger contractions. The $[Ca^{2+}]_i$ oscillations in these cells were insensitive to nifedipine, but readily inhibited by the T-type Ca^{2+} channel inhibitor NNC55-0396. In conclusion, our data suggest that the spread of $[Ca^{2+}]_i$ signals in human myometrium is achieved *via* propagation of long-lasting action potentials. The propagation was fast when action potentials propagated along bundles of myocytes and slower when propagating between the bundles of uterine myocytes.

Keywords: calcium signalling • human myometrium • uterine contractility • spontaneous activity • calcium channel inhibitors

Introduction

Coordinated activity of smooth muscle is important for proper functioning of many systems in human body. In the reproductive system, smooth muscle contractility is involved in every step of the reproductive process, from conception to delivery. The precise timing and coordination of uterine contractions during labour are essential for successful childbirth. Premature onset of uterine activity may lead to preterm labour, whereas weak and unsynchronized contractions (uterine dystocia) often result in prolonged labour, caesarean section and/or postpartum haemorrhage. To understand the pathogenesis of dysfunctional labour, we need to understand the physiological mechanisms that trigger and regulate myometrial contractions. In the myometrium, as in other types of phasic smooth muscle, contractions are triggered by action potentials on the surface membrane [1–3]. Myometrial action potentials have complex waveforms, which fall into one of two categories: plateau-type or burst-type [3–6]. Both types of action potential occur spontaneously and propagate between myocytes *via* specialized low-resistance intercellular channels called gap junctions. The fundamental role of gap junctions for propagation of myometrial electrical activity has been well documented in the literature [7, 8]. During pregnancy progression, the number of gap junction plaques between neighbouring myocytes progressively increases leading to improved electrotonical coupling between individual cells [9]. Improved electrotonical coupling allows the action potentials to spread and engulf the entire uterus leading to synchronized contractions during labour. Interestingly, the capacity of human myometrial

*Correspondence to: Anatoly SHMYGOL,
Division of Reproductive Health,
Warwick Medical School,
Clifford Bridge Road,
Coventry, UK, CV2 2DX.
Tel.: (+44)02476968702
Fax: (+44)02476968653
E-mail: a.shmygol@warwick.ac.uk

doi: 10.1111/j.1582-4934.2012.01626.x

tissues to develop gap junctions is retained *in vitro* for up to 48 hrs and may depend on the activity of cyclooxygenase or lipoxygenase pathways [10].

To date, the mechanisms underlying the spontaneous generation of action potentials (myometrial autorhythmicity) have not been fully elucidated. Enzymatically dissociated human myometrial cells rarely show spontaneous activity suggesting that myometrial autorhythmicity may represent an emergent property of the cellular network [11]. Indeed, the cellular composition of human myometrium is non-homogeneous: there are at least two major cell types; typical contractile myocytes and non-contractile interstitial Cajal-like cells [12, 13] in addition to populations of uterine fibroblasts and invading leucocytes. The interstitial Cajal-like cells, recently rebranded as uterine telocytes [14], have been proposed to contribute to myometrial autorhythmicity although this suggestion was based on indirect evidence *i.e.* inhibition of myometrial contractions by a non-competitive KIT inhibitor imatinib-mesylate [15]. Double-impalement microelectrode recordings from the telocytes and smooth muscle cells would provide definitive evidence for the involvement of telocytes in autorhythmicity, but this has not yet been achieved in the myometrium. Cellular heterogeneity and complex geometry of the myometrium are important determinants of the relationship between $[Ca^{2+}]_i$ dynamics and mechanical behaviour of the uterus [16, 17]. The relationship between $[Ca^{2+}]_i$ and force in human myometrium has been investigated by several groups using surface fluorimetry combined with mechanography in strips loaded with ratiometric Ca^{2+} sensitive dyes Fura-2 [18–21] or Indo-1 [22, 23]. When properly calibrated, these measurements can provide quantitative data on the '$[Ca^{2+}]_i$ – force' relationship. However, the surface fluorimetry gives a spatially averaged signal with no information on cellular distribution of $[Ca^{2+}]_i$. Spatial information on $[Ca^{2+}]_i$ wave propagation within and between individual cells has been obtained in confluent cultures of primary human uterine myocytes [24] and immortalized myometrial cell lines [25]. Although useful, these experimental models are not ideal because the enzymatic cell isolation can result in unintended selection of one cell type over another and because of phenotypic transition in cultured cells can potentially distort the profile of $[Ca^{2+}]_i$ signals compared to that *in situ*.

To date, the spatio-temporal characteristics of tissue-level $[Ca^{2+}]_i$ transients have only been investigated in rat myometrium [26]. It remains unknown how human myometrial $[Ca^{2+}]_i$ signals are organized in space and time. The purpose of this study was to elucidate the spatio-temporal properties of tissue-level $[Ca^{2+}]_i$ signals in intact human myometrium. Performed with confocal imaging of thin slices of uterine tissue loaded with Ca^{2+}-sensitive dye, we were able to visualize the dynamics of $[Ca^{2+}]_i$ over relatively large areas of spontaneously contracting human myometrium. Thus, for the first time, we provide information on the time course of $[Ca^{2+}]_i$ transients in individual cells within tissue slice and relate this to the time course of tissue-level $[Ca^{2+}]_i$ transients and contractions.

Materials and methods

Tissue procurement and slice preparation

Myometrial biopsy specimens were obtained with informed written consent (information leaflet Ref: PTL220705) and approval from the Local Ethics Committee at University Hospital Coventry and Warwickshire (REC-05/Q2802/107) from term-pregnant women ($\geq$37 weeks gestation) undergoing elective caesarean section before the onset of labour.

Myometrial specimens were collected into sterile 25 ml plastic tubes filled with cold Krebs solution, placed on ice and delivered to the laboratory within 20–30 min. On arrival, each biopsy specimen was trimmed under a stereo microscope into a strip of approximately 1.0 $\times$ 0.5 $\times$ 0.3 cm. The strip was then ligatured with braided 2-0 Mersilk suture (Ethicon, Inc., Kirkton, UK) at both ends before being stretched and fixed to the base of a stainless steel tissue holder using cyanoacrylate glue. From this, 200 μm-thick slices were cut using an oscillating vibroslicer (Integraslice 7550 PSDS; Campden Instruments, Loughborough, UK) in oxygenated ice-cold Krebs solution. Slicing was performed with razor blades at an oscillating speed of 86 Hz with lateral amplitude of 1 mm and an advance speed of 0.10–0.20 mm/sec. First cuts and the glued base of the strip were discarded. Each slice was then separated by cutting the extremity of the slice using fine dissecting scissors and transferred into Krebs solution. After 1 hr incubation at room temperature for equilibration and recovery and 30 min. loading with Fluo-4/AM (see below) slices were used in experiments within 4–6 hrs. Microscopic examination of loaded slices revealed either a single bundle of several hundreds of myocytes or two to three bundles of myocytes separated by interstitial space.

Confocal imaging of $[Ca^{2+}]_i$

For $[Ca^{2+}]_i$ recording, slices were incubated for 30 min. at 37°C in Krebs solution containing 13 μM Fluo-4/AM (Invitrogen, Paisley, UK). Non-ionic detergent Pluronic F127 (0.025%, w/v) was included to aid the dye loading. This protocol produced homogeneous staining of cells throughout the slice and gave better tissue viability compared to loading at room temperature, which required up to 4 hrs incubation to achieve the same intensity of Fluo-4 signal. The loaded slice was placed in a glass-bottomed Petri dish and weighted down with a 250 mg slice grid (HSG-5; ALA Scientific, Farmingdale, NY, USA). The dish was then secured in a spring-loaded holder in a temperature-controlled environmental chamber on the stage of an inverted microscope (Axiovert 200 M; Carl Zeiss, Cambridge, UK) equipped with an LSM 510 META confocal scanner (Carl Zeiss) and

Table 1 Incidence of myometrial strips and thin slices showing different types of spontaneous activities

	Burst-type activity	Plateau-type activity	Desynchronized activity	No spont. activity
Strips	31	33	9	4
Slices	15	12	5	7

superfused with pre-warmed (35°C) Krebs solution at a flow rate of 2 ml/min. for 30–40 min. until stable spontaneous contractions developed. Slices that failed to develop spontaneous activity within this timeframe were excluded (see Table 1 for numbers).

Confocal imaging of Fluo-4 loaded slices was achieved by scanning a 488 nm wavelength laser beam focussed into a diffraction-limited spot *via* a Fluar 5x/0.25NA objective lens and recording fluorescence through a band-pass filter (505–530 nm) using a photomultiplier tube with a pinhole in front of it. The pinhole diameter was set to 2 Airy units to reject most of the out-of-focus fluorescence and to maximize the throughput of light originating from the focal plane. The excitation and emission beams were separated by a dichromatic mirror centred at 495 nm. The signal from the photomultiplier was digitized to yield 512 pixels per line and 256 lines were scanned per one frame giving the frame size of 512 × 256 pixels. By reducing the number of scan lines to 256 we were able to acquire images at rates of two to four per sec. with unidirectional and bidirectional scan. The use of low-magnification objective lens allowed imaging of a large area measuring 1.8 × 0.9 mm. Superior light-gathering ability of the high numerical aperture objective lens used in our study was crucial for ensuring a good signal to noise ratio even at lowest intensity of laser illumination. Keeping the intensity of illumination at low level was critical for preventing photobleaching during prolonged recordings. The image acquisition was controlled using Zeiss LSM v4.0 software. Time series of up to 8000 frames were collected and stored on a hard drive for off-line analysis.

Image analysis

The LSM files were imported into ImageJ (NIH; http://imagej.nih.gov/ij/) using the LSM Toolbox plug-in (http://imagejdocu.tudor.lu/doku.php?id=plugin:inputoutput:lsmtoolbox:start).

Figure 1 illustrates the procedure used to extract time series data from the image stacks. For each data file, a maximum intensity projection was calculated to aid the visualization of individual cells and to identify the area of most pronounced movement of the slice edge, which was then used to monitor the time course of contractions (see below). The maximum intensity projection image was used to draw regions of interest (ROI) encompassing either individual cells (single-cell ROI) or groups of 10–50 cells (multi-cell ROI). The ROI Manager in ImageJ was used to create a list of ROIs. This list was then applied to the original image stack and the Multi-Measure function in the ROI Manager was used to extract the intensity profiles over time for each ROI. The ROI intensity profiles were imported into OriginPro 8.0 (OriginLab Corporation, Northampton, MA, USA) for further processing, graphing and statistical analysis. The intensity *versus* time profile from each ROI was plotted (Fig. 1 Ba). Even at a low intensity of laser illumination there was a small decrease in the baseline indicating that some photobleaching was still taking place. To correct for this, a baseline connecting the lowest values of fluorescence between successive contractions was drawn and each trace was normalized to its corresponding baseline to yield a photobleaching-corrected self-ratio trace (F/F_0). F/F_0 was then used as a measure of $[Ca^{2+}]_i$ [27]. This is illustrated in Fig. 1 Bb where resting $[Ca^{2+}]_i$ corresponds to $F/F_0 = 1$ and upward deflections indicate an increase in $[Ca^{2+}]_i$.

To monitor the time course of contraction, a larger ROI was placed over the moving edge of the slice (*e.g.* ROI 5 in Fig. 1 Aa). The mean intensity obtained from this ROI (black trace in Fig. 1 Ba) is proportional to the displacement of the slice as it moves in and out of the ROI during the contraction-relaxation cycle. The displacement trace was normalized

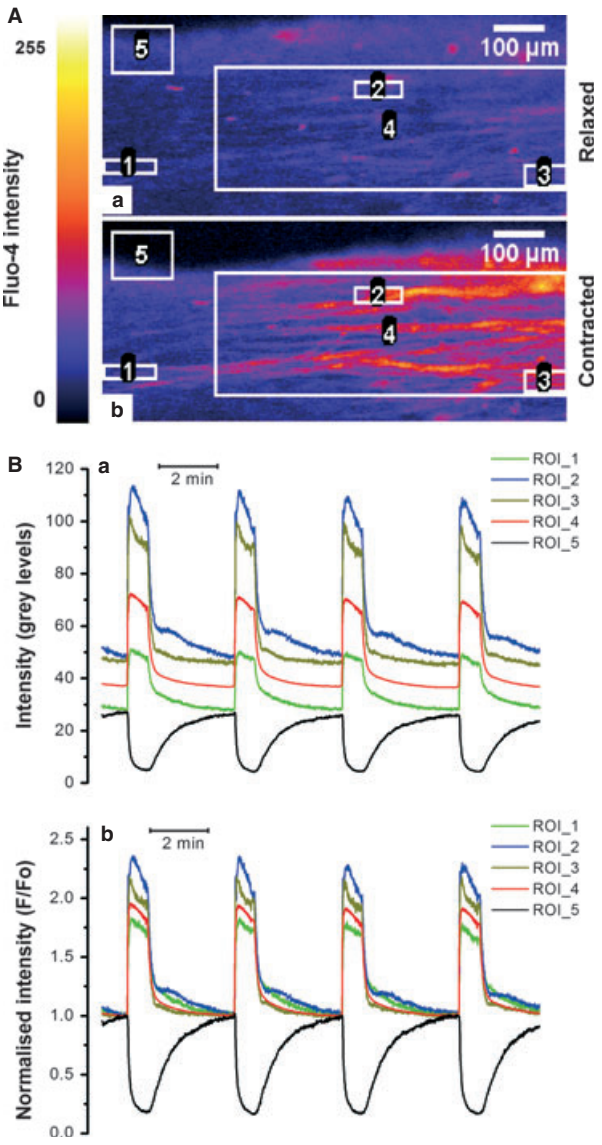

Fig. 1 Confocal imaging of spontaneous $[Ca^{2+}]_i$ transients and contraction in thin slices of human myometrium. (**A**) Raw fluorescence images of Fluo-4 loaded myometrial slice in the relaxed and fully contracted state show the arrangement of regions of interest (ROIs) for extraction of the intensity *versus* time data: single-cell ROIs (ROI 1-3), multi-cell ROI (ROI 4) and a contraction-monitoring ROI (ROI 5) are shown. (**B**) Intensity *versus* time traces extracted from the ROI. (**Ba**) Raw data; (**Bb**) Normalized intensity showing repetitive increases in $[Ca^{2+}]_i$ (red, blue, green and olive traces) and the slice edge displacement indicative of contraction (black trace).

to the highest values of intensity between contractions, when the slice was fully relaxed. The relaxed state therefore corresponds to $F/F_0 = 1$ and downward deflections follow the time course of contractions. Although a similar approach is routinely used by many authors for monitoring contractions of cardiac myocytes simultaneously with $[Ca^{2+}]_i$ it has to be

kept in mind that edge displacement technique reflects isotonic contraction and their time course may not necessarily be the same as that of isometric contractions measured in an organ bath.

Organ bath experiments

The strips measuring approximately 2 × 2 × 10 mm (with muscle fibres running along the long axis) were cut from myometrial biopsies with a scalpel blade. Each strip was then mounted vertically in the LSI Letica four-channel organ bath (ADInstruments Ltd, Oxford, UK) with one end tied with braided 2-0 Mersilk suture to a stainless steel hook and the other to an isometric force transducer (Type MLT0201/D) attached to a single-axis manipulator. Each organ bath chamber was filled with 10 ml of Krebs solution. The strips were stretched to 20 mN passive tension and incubated at 37°C for 2 hrs to equilibrate. During the equilibration period and throughout the experiment, the Krebs solution was changed every hour by empting and refilling the chambers using electronically controlled valves. In most cases, stable spontaneous contractions developed within 40–90 min. Those strips that did not show spontaneous contractions after 2 hrs were excluded from further experimentation (see Table 1 for numbers).

Chemicals and solutions

The Krebs solution used in our experiments contained (in mM): NaCl, 133; KCl, 4.7; $MgSO_4$, 1.2; KH_2PO_4, 1.2; Glucose, 11.1; TES (*N*-[tris(hydroxymethyl)methyl]-2-aminoethanesulfonic acid), 10; $CaCl_2$, 1.25; pH adjusted to 7.4 with NaOH. In the organ bath experiments, 25 mM $NaHCO_3$ was used in place of TES and pH was maintained at 7.4 by continuous bubbling of solution with 5% CO_2. All chemicals used in this study were purchased from Sigma-Aldrich (Dorset, UK), except for Fluo-4/AM which was from Invitrogen and the T-type Ca^{2+} channel inhibitor NNC55-0396, which was supplied by Tocris Bioscience (Bristol, UK).

Statistics and data presentation

Where appropriate, statistical significance was tested using two-tailed Student's *t*-test with *P* values below 0.05 considered sufficiently low to reject the null hypothesis. Evaluation of inhibitory action of NNC55-0396 was performed with paired Student's *t*-test with each slice serving as its own control. Statistical calculations were performed in OriginPro 8.0 data analysis and graphing software, which was also used for preparation of the figures. Numerical values of measured parameters are expressed as means ± standard error of mean with *n* values referring to the number of myometrial samples used.

Results

Relationship between single-cell and tissue-level $[Ca^{2+}]_i$ transients

Confocal imaging of $[Ca^{2+}]_i$ in thin slices of human myometrium enabled the investigation of the relationship between tissue-level $[Ca^{2+}]_i$ transients during spontaneous contractions and individual-cell $[Ca^{2+}]_i$ transients. Figure 1A illustrates the arrangement of single-cell ROIs (ROI 1-3), multi-cell ROI (ROI 4) and a contraction-monitoring ROI (ROI 5) in a typical slice at rest (Fig. 1Aa) and at the peak of contraction (Fig. 1 Ab). The absolute values of fluorescence intensity recorded from single-cell ROIs (Fig. 1Ba) varied substantially between individual ROIs presumably reflecting the differences in the Fluo-4 loading of individual cells, although a variation in the true amplitude of $[Ca^{2+}]_i$ rises in individual cells could not be ruled out. Indeed, normalization of the Fluo-4 signal to its resting level (F/F_0), a procedure that compensates for the cell-to-cell variation in dye loading, decreased but did not abolish the variations in F/F_0 transient amplitude, suggesting that there was a true variation in peak values of $[Ca^{2+}]_i$ between individual cells (Fig. 1 Bb). This finding is in agreement with previously described cell-to-cell variation in the density of the Ca^{2+} channel currents recorded under voltage clamp [28].

Within limits of resolution, the timing and duration of $[Ca^{2+}]_i$ transients were very close in all cells within a bundle. That is, the time of onset and the duration of the individual-cell $[Ca^{2+}]_i$ transients (ROI 1-3 in Fig. 1 A, corresponding to green, blue and olive traces in Fig. 1 B) coincided with that recorded from the entire bundle (ROI 4 in Fig. 1 Aa corresponding to the red trace in Fig 1B) indicating virtually simultaneous activation of cells within the bundle.

As illustrated in Figure 2, there was a similarity of appearance between the waveforms of contractions recorded from the full-size strips in organ bath and from bundles of myocytes in thin slices under the microscope. In agreement with data published by other researchers [3, 6], the waveform of isometric contractions in our organ bath experiments resembled one of the two major types: the tetanus-like contractions (Fig. 2 Ab) or the smooth mono-phasic contractions (Fig. 2 Aa), triggered by the burst-type and plateau-type action potentials respectively. In the former case, the total force developed during any particular E-C cycle resulted from fusion of twitches triggered by the individual spikes in the burst. Consequently, the first derivative of contractile force (dF/dT, bottom trace in Fig. 2 Ab) exhibited multiple positive peaks, whereas the first derivative of the plateau-type contraction had a single positive peak (bottom trace in Fig. 2 Aa). As a result, the plateau-type contraction reached its peak earlier compared to the burst-type, where force continued to rise until the end of the contractile cycle. Likewise, the edge displacement reached its peak earlier in slices exhibiting the plateau-type $[Ca^{2+}]_i$ transients (Fig. 2 Ba) than in those with the burst-type activity (Fig. 2 Bb). The plateau-type activity was characteristic of just under one-half of myometrial slices (12 of 27 slices), whereas the remainder exhibited burst-type $[Ca^{2+}]_i$ transients. The frequency of spontaneous contractions was higher in thin slices compared to the standard-size myometrial strips: 4.46 ± 0.6 mHz ($n = 27$) in slices and 1.88 ± 0.1 ($n = 64$) in strips ($P < 0.05$, two-tailed unpaired *t*-test). The duration of the $[Ca^{2+}]_i$ transients in thin slices, measured as full width at half-magnitude (FWHM), was significantly shorter compared to the FWHM of isometric contractions recorded in organ bath experiments: 37.8 ± 4.2 sec. ($n = 27$) *versus* 52.5 ± 1.9 sec. ($n = 64$, $P < 0.05$, two-tailed unpaired *t*-test).

The virtually synchronous onset of $[Ca^{2+}]_i$ transients in individual cells within a bundle of myocytes observed in the above experiments

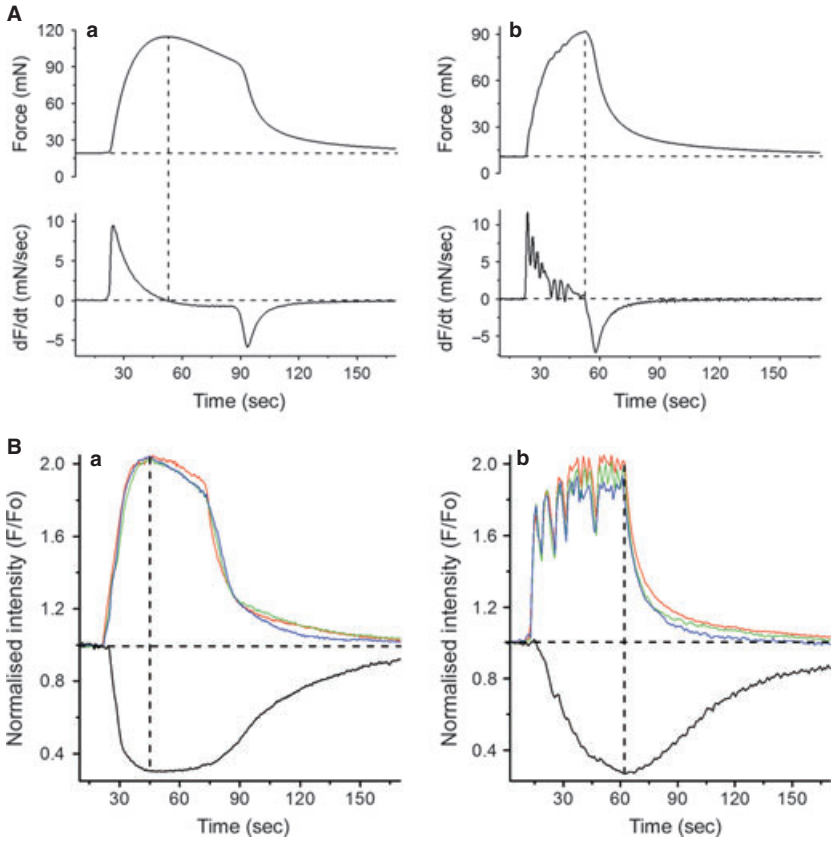

Fig. 2 Comparison of the waveforms of isometric contractions recorded in organ bath and $[Ca^{2+}]_i$ transients and isotonic twitches recorded from the thin slices of myometrium. (**A**) Isometric force (upper trace) and its first derivative (lower trace) recorded from strips exhibiting the plateau-type (**Aa**) or burst-type (**Ab**) activity. The main difference between these two types was the position of the peak force: it occurred earlier in strips with plateau-type activity and was followed by a slow decay of force before the rapid relaxation at the end of the contraction-relaxation cycle. In the burst-type strips, contractile force continued to rise until the end of the contraction-relaxation cycle. The rising phase of contraction had a 'rugged' appearance, more evident in the first derivative trace. (**B**) $[Ca^{2+}]_i$ transients (red, blue and green traces from multi-cell ROIs positioned at opposite ends of the viewing field) and isotonic contractions (black traces) recorded from two different slices, one exhibiting the plateau-type (**Ba**) and another the burst-type (**Bb**) activity. In both cases, the ROIs were positioned over cell groups belonging to a single bundle of myocytes present in each slice. The burst-type $[Ca^{2+}]_i$ transient had a 'rugged' appearance that resulted from a fusion of many individual increments in $[Ca^{2+}]_i$ presumably corresponding to repetitive spikes in the burst-type action potential, whereas the plateau-type $[Ca^{2+}]_i$ transient has a smooth appearance. Vertical dashed lines in all panels indicate the peaks of contraction.

is compatible with the idea that during each E-C cycle, the myocytes are recruited by a rapidly propagating action potential rather than by a slow-spreading intercellular $[Ca^{2+}]_i$ wave (cf.[29]).

Synchronicity and propagation of tissue-level $[Ca^{2+}]_i$ transients

To investigate the propagation of $[Ca^{2+}]_i$ transients between cells within a myometrial bundle, we superimposed the $[Ca^{2+}]_i$ traces from three single-cell ROIs positioned along the longitudinal axis of a single bundle of myocytes (Fig. 3b) or transversely, perpendicular to the axis (Fig. 3a). The onset of $[Ca^{2+}]_i$ transients in cells along and across a particular bundle was simultaneous, indicating that the propagation time in either direction was shorter than the time interval between successive frames. In contrast, propagation between the bundles was substantially slower resulting in the measurable time delays between $[Ca^{2+}]_i$ transients in separate bundles of myocytes. This is illustrated in Figure 4 where two sets of longitudinally and transversely oriented ROIs were positioned over two separate bundles. Graphs a and b in Figure 4 show that cells within each bundle were activated simultaneously in either the longitudinal or transversal direction, similar to that shown in Figure 3. However, there was a 1 sec. time delay in the $[Ca^{2+}]_i$ transient onsets between the two bundles. The averaged latency of $[Ca^{2+}]_i$ transient propagation between the bundles was 0.75 ± 0.5 sec. in slices obtained from seven different samples.

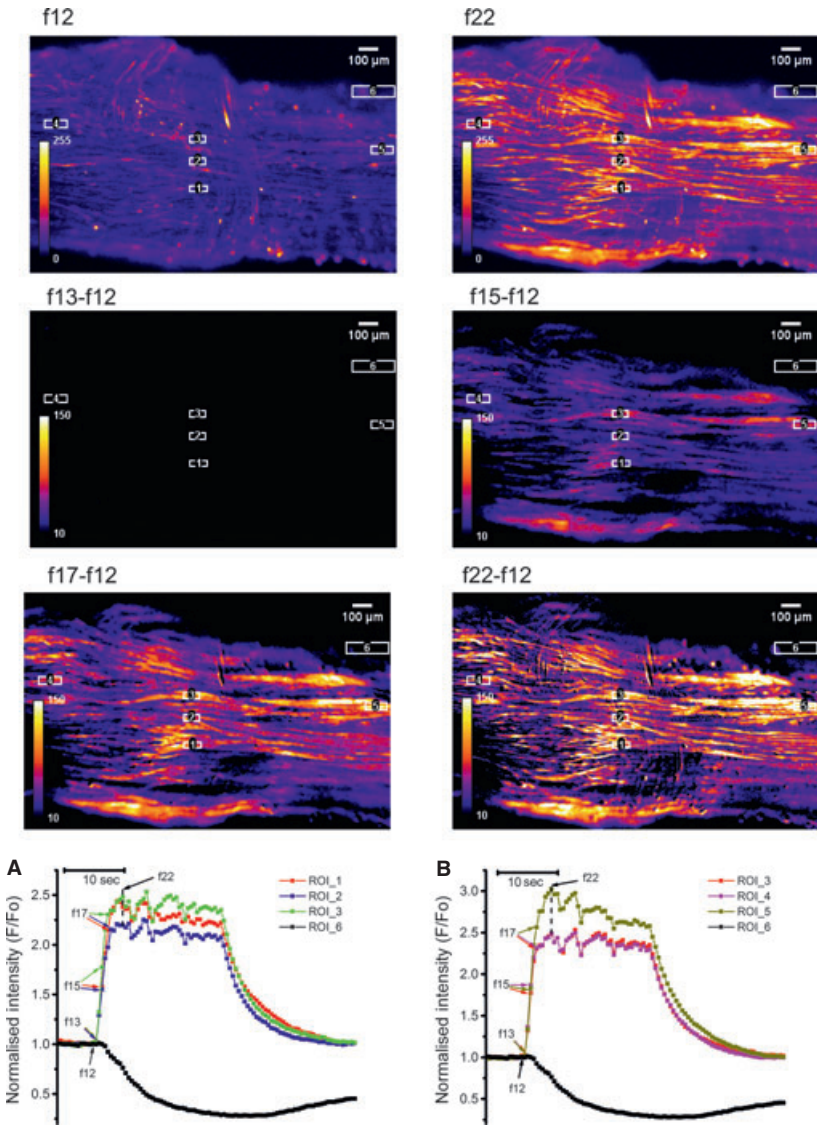

Fig. 3 Synchronous activation of myocytes in myometrial slice containing a single bundle of myocytes. Frames in top row show a Fluo-4 loaded slice at rest (f12) and at peak of $[Ca^{2+}]_i$ transient (f22). The 'resting fluorescence' frame (f12) was subtracted from subsequent frames during the rising phase of $[Ca^{2+}]_i$ transients to yield the 'delta F' images where cells are visible only when they rise $[Ca^{2+}]_i$ above the resting level. The ROI were positioned along the longitudinal axis (ROI 4, 3 and 5) or perpendicular to it (ROI 1-3). Graph in (**a**) shows $[Ca^{2+}]_i$ traces extracted from ROIs positioned in longitudinal direction. Graph in (**b**) shows $[Ca^{2+}]_i$ traces extracted from ROIs positioned perpendicular to the longitudinal axis. Black traces correspond to a contraction-monitoring ROI 6. Arrows next to frame numbers in both graphs indicate data points corresponding to the corresponding frames shown above. Note that $[Ca^{2+}]_i$ transient spread between cells in both sets of ROIs without measurable delay indicating synchronous activation of cells in both directions.

Although the majority of myometrial preparations produced contractions of constant amplitude, a proportion of both, the regular-size strips and the thin slices of myometrium, exhibited contractions of alternating amplitude (illustrated in Fig. 5A and B). Such contractions were observed in 9 of 64 strips and in 5 of 27 thin-slice preparations. Closer examination of these contractions and especially their first derivative (lower trace in Fig. 5A) revealed that the alternating amplitude of contractions in some strips may be due to a recurrent coincidence of contractions in several disconnected bundles contracting at their own frequencies. Recordings of $[Ca^{2+}]_i$ transients from two separate bundles in a slice exhibiting similar alternating contractions revealed the lack of synchronization between these bundles (Fig. 5B). A larger amplitude of the edge displacement (black trace in Fig. 5B) was observed when $[Ca^{2+}]_i$ transients was generated in both bundles

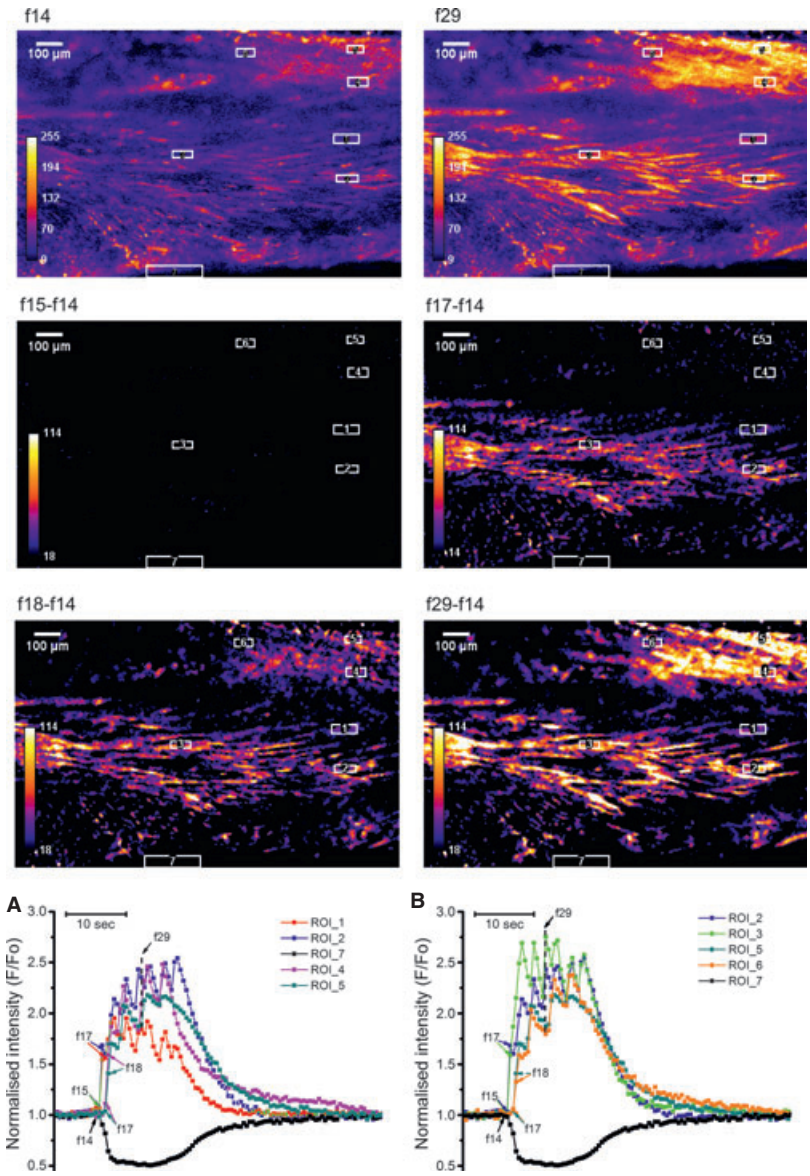

Fig. 4 Propagation of $[Ca^{2+}]_i$ transient in myometrial slice containing two bundles of myocytes, one in the middle, another in the top right corner. Data presentation is similar to that in Figure 3 with the exception that two sets of three ROIs were used in this experiment: ROI 1-2 and ROI 4-5 to measure propagation perpendicular to the longitudinal axis in each bundle and ROI 2-3 and ROI5-6 to measure propagation in axial direction. In this experiment, there was a 1 sec. time delay between the onset of $[Ca^{2+}]_i$ transients in neighbouring bundles but cells within each bundle were activated simultaneously. Typical of seven experiments on slices from seven different samples.

at the same time. All five slices that exhibited this kind of activity contained at least two visibly unconnected bundles of myocytes. The $[Ca^{2+}]_i$ transients in desynchronized bundles were similar in shape between bundles and resembled either burst-type or plateau-type activity akin to that observed in slices with synchronized bundles. The only difference was that, in desynchronized slices, the $[Ca^{2+}]_i$ transients generated at different frequencies periodically coincided, thus giving rise to contractions of alternating amplitude. Individual cells within each of these bundles produced $[Ca^{2+}]_i$ transients whose timing and duration were characteristic of their respective bundle suggesting that de-synchronization occurred between the bundles, but not between the individual cells belonging to the same bundle. This is illustrated in Figure 5C where red and orange traces correspond to two individual cells within one bundle and blue and violet

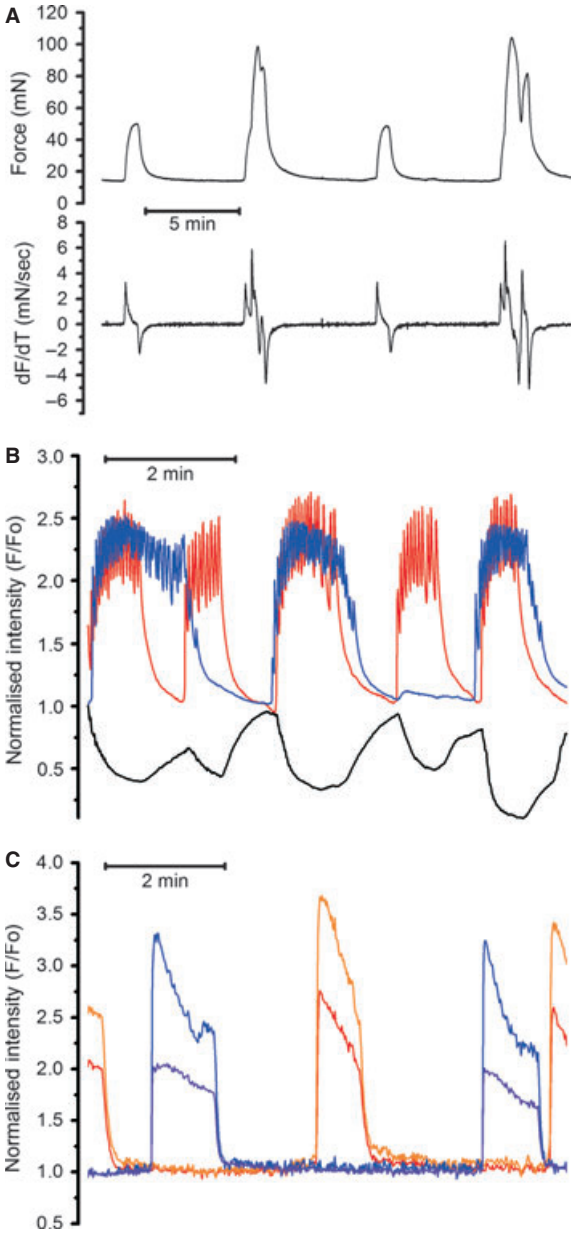

Fig. 5 Desynchronized $[Ca^{2+}]_i$ transients elicit contractions of alternating amplitude. (**A**) Example of alternating isometric force (upper trace) and its first derivative (lover trace) recorded from a strip in an organ bath experiment (typical of 23 recordings from 23 different samples). (**B**) Multi-cell $[Ca^{2+}]_i$ transients showing no synchronization (typical of five other slices from five different samples). Red and blue traces correspond to ROI positioned over two different bundles. Note that larger contractions occurred when $[Ca^{2+}]_i$ transients in different bundles coincided (marked by asterisks). (**C**) Single-cell ROIs positioned over two different cells in one bundle (red and orange traces) and two more cells in another bundle (blue and violet traces) in a slice with desynchronized bundles. Note that the $[Ca^{2+}]_i$ transients in individual cells within each bundle remained synchronized.

traces correspond to two individual cells in a neighbouring desynchronized bundle. It is obvious that there was good synchronization between cells in each bundle, whereas bundles themselves were completely asynchronous.

Although the majority of cells within the bundle remained quiescent between the global synchronized $[Ca^{2+}]_i$ transients, some cells were producing low-amplitude $[Ca^{2+}]_i$ oscillations (illustrated in Fig. 6). This desynchronized oscillatory behaviour was observed in 18 of 27 slices regardless of the type of global $[Ca^{2+}]_i$ signals (compare Fig. 6A, the burst-type and Fig. 6B, the plateau-type of tissue-level activity). In contrast to the global $[Ca^{2+}]_i$ signals, which always triggered contractions, the individual-cell $[Ca^{2+}]_i$ oscillations were not accompanied by any measurable contractions (black traces with downward deflections in Fig. 5A and B). The oscillating cells varied greatly in both their shape and size, from small rounded through stellate to very large elongated shapes. The $[Ca^{2+}]_i$ oscillations generated by these cells never spread to the neighbouring cells, although the global tissue-level $[Ca^{2+}]_i$ transients did engulf the cytoplasm of oscillating cells indicating that they were electrically coupled with the rest of the cellular network.

Effect of Ca^{2+} channel blockers on tissue-level and localized $[Ca^{2+}]_i$ transients

In human myometrium, low micromolar concentrations of nifedipine, a dihydropyridine-family Ca^{2+} channel inhibitor produce complete inhibition of the L-type Ca^{2+} channels without affecting the low voltage-activated (T type) Ca^{2+} channels [28]. In our experiments, an application of 1 μM nifedipine immediately abolished the tissue-level $[Ca^{2+}]_i$ transients in 18 slices of 18 tested ones, but did not affect the asynchronous $[Ca^{2+}]_i$ oscillations in 10 of 11 slices where oscillating cells were present (illustrated in Fig. 6C). The resistance of $[Ca^{2+}]_i$ oscillations to nifedipine indicates that non-L-type Ca^{2+} channel, *e.g.* T type, might be involved. To test this possibility, we used (1S,2S)-2-[2-(*N*-[(3-benzoimidazol-2-yl)propyl]-*N*-methylamino)ethyl]-6-fluoro1,2,3,4-tetrahydro-1-isopropyl-2-naphtyl cyclopropanecarboxylate dihydrochloride (NNC 55-0396), a non-hydrolyzable derivative of mibefradil with improved selectivity towards the T-type Ca^{2+} channels [30, 31]. We tested this compound in nine thin slices, eight of which contained asynchronous oscillating cells. As illustrated in Figure 6D, the application of 10 μM NNC-55 0396 caused complete inhibition of localized asynchronous $[Ca^{2+}]_i$ oscillations indicating that the T-type Ca^{2+} channels were involved in the single-cell asynchronous $[Ca^{2+}]_i$ oscillations. The tissue-level $[Ca^{2+}]_i$ transients were not abolished in the presence of NNC-55 0396, although their amplitude and frequency were significantly decreased: the amplitude was reduced from 2.19 ± 0.16 F/F_0 to 1.68 ± 0.12 F/F_0 and the frequency (calculated over 10 min. periods before and after the addition of NNC-55 0396) was slowed from 4.32 ± 0.71 to 3.02 ± 0.38 mHz ($P < 0.05$, $n = 9$, paired Student's *t*-test). The duration of the tissue-level $[Ca^{2+}]_i$ transients (measured as FWHM) was shortened from 29 ± 4 to 18 ± 4 sec. in the presence of NNC-55 0396 ($P < 0.05$, $n = 9$, paired

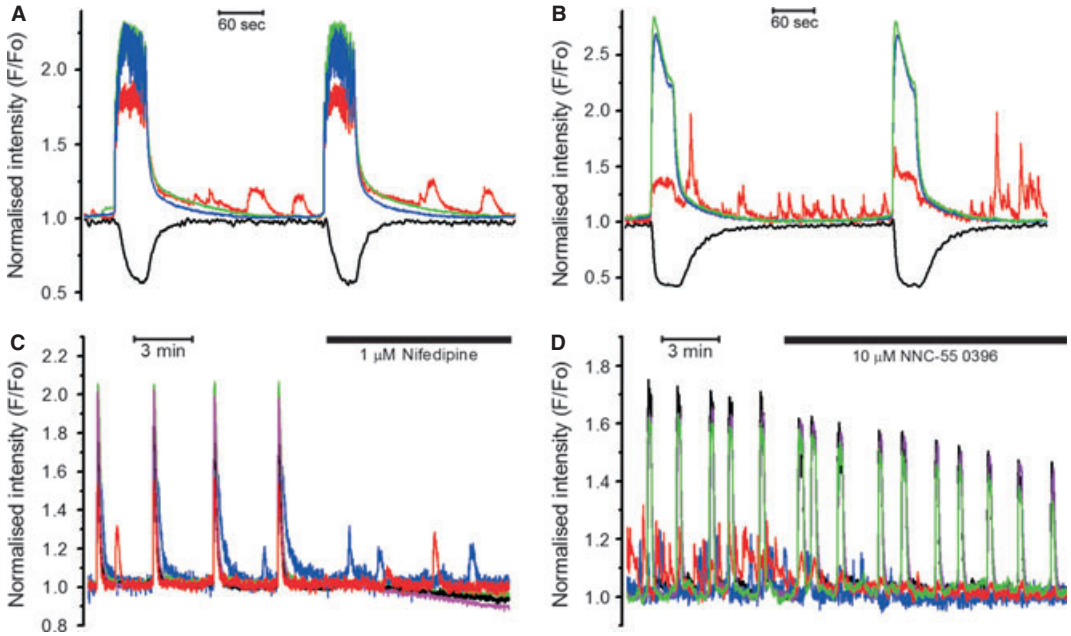

Fig. 6 Oscillating cells in myometrial slices (observed in 18 of 27 slices). Unsynchronized, low-amplitude $[Ca^{2+}]_i$ oscillations (red trace) in a burst-type (**A**) and plateau-type (**B**) slices. Note that only tissue-level $[Ca^{2+}]_i$ transients (blue and green traces in both graphs) were capable of triggering contractions (black traces). (**C**) Nifedipine inhibited tissue-level $[Ca^{2+}]_i$ transients, but not $[Ca^{2+}]_i$ oscillations in desynchronized cells. (**D**) $[Ca^{2+}]_i$ oscillations were inhibited by NNC-55 0396, a specific T-type Ca^{2+} channel inhibitor.

Student's *t*-test). These data indicate that the T-type Ca^{2+} channels were critically important for the asynchronous $[Ca^{2+}]_i$ oscillations and were also contributing to the pacemaking mechanism because their inhibition slowed the frequency of spontaneous contractions.

Discussion

In the present study, we have characterized the spatio-temporal properties of the tissue-level $[Ca^{2+}]_i$ transients using confocal microscopy and thin slices of intact human myometrium. Myometrial slices exhibited stable spontaneous $[Ca^{2+}]_i$ transients and contractions for at least 30 min. of continuous recording on the confocal microscope suggesting that prolonged low intensity laser illumination, as used in our experiments, had no detrimental effect on the tissue. We found that the waveform of $[Ca^{2+}]_i$ transients and isotonic contractions recorded from thin slices was similar to the waveform of isometric contractions recorded from the larger strips in traditional organ bath experiments, suggesting that the spatio-temporal information obtained from thin slices is representative of the whole tissue. These results validate our experimental approach and also lend support to the idea that a single myocyte is not the smallest functional unit of the myometrium. Our data suggest that a myometrial fasciculus, that is, a structure encompassing several bundles of myocytes should be considered the minimal functional unit of the myometrium (cf. [29]). The dissimilarity of the contraction frequencies and durations in full-size strips and thin slices may indicate that the total number of myocytes, telocytes and fibroblasts involved in the E-C cycle is important for setting the duration and frequency of spontaneous activity.

In the labouring uterus, a very large number of myocytes forming a complex geometrical structure of myometrium has to contract in synchrony to increase the intrauterine pressure sufficiently high to dilate the cervix and eventually expel the foetus through the birth canal. During each contraction-relaxation cycle, the peak of myometrial force is reached within 15–20 sec. in strips exhibiting the plateau-type action potentials or 40–60 sec. in strips exhibiting the burst-type activity [3, 6]. To account for the relatively slow kinetics of force development in human myometrium, it has been suggested that the rising phase of contraction is due to a relatively slow progressive recruitment of the myocytes into the contractile state [29, 32, 33]. The slow recruitment of myocytes into the contractile state has been explained by the 'action potential – calcium wave' hypothesis, which postulates that action potentials propagate along the myometrial bundles and trigger $[Ca^{2+}]_i$ transients only in myocytes of the outer layer of the bundle; the rest of the myocytes within any particular bundle are recruited by concentric intercellular $[Ca^{2+}]_i$ waves propagating perpendicular to the bundle axis [29, 33]. Our thin slice technique allowed us to test this hypothesis experimentally for the first time. If the recruitment of the cells in a perpendicular direction was due to concentrically spreading intercellular $[Ca^{2+}]_i$ waves, one would expect to observe a time delay in the onset of the $[Ca^{2+}]_i$ transients between cells in transversal direction. In contrast, we found that all cells within the bundle were activated virtually simultaneously, in less than

0.25 sec., and $[Ca^{2+}]_i$ remained at high levels for the entire duration of the E-C cycle (see Figs 3 and 4). This is compatible with the idea that the recruitment of cells within the bundle was due to rapid propagation of the long-lasting action potentials throughout the entire bundle. Propagation between the bundles, on the other hand, was measurably slower. Latencies as long as 2 sec. (0.75 ± 0.5 sec. on average) were observed suggesting that a slow recruitment of myometrial bundles rather than individual myocytes was underlying the slow rise of luminal pressure recorded by intra-uterine catheter (cf.[33]).

In five of 27 slices, we observed no propagation between the neighbouring bundles at all. Instead, the $[Ca^{2+}]_i$ transients in each bundle were generated independently, at their own frequencies. This was accompanied by alternating contractions, *i.e.* larger contractions occurred when the $[Ca^{2+}]_i$ transients in neighbouring bundles coincided. Importantly, even in these decoupled bundles, all cells within the same bundle were generating $[Ca^{2+}]_i$ transients of identical duration and without measurable latencies lending additional support to the idea that the $[Ca^{2+}]_i$ signal propagation in the myometrium was mediated solely by the long-lasting action potentials. Relatively slow rate of propagation between the bundles is likely due to a higher resistance of the 'connecting bridges' [17]. They may represent the 'weakest link' responsible for the failure of proper coordination of myometrial contractions in labour dystocia.

Almost 70% of thin slices of human myometrium contained cells producing continuous low-amplitude $[Ca^{2+}]_i$ oscillations between the global tissue-level $[Ca^{2+}]_i$ transients. These oscillations were insensitive to nifedipine, but sensitive to the T-type Ca^{2+} channel inhibitor NNC-55 0396 suggesting that the T type was the predominant voltage-activated Ca^{2+} channel in the oscillating cells. In many types of smooth muscle, T-type Ca^{2+} channels are involved in a vast variety of cellular functions such as pacemaking, proliferation, contraction, etc. [28, 34–37]. An increase in the T-type Ca^{2+} channel expression has been described in proliferating pulmonary artery myocytes [35]. Likewise, the oscillating cells observed in our experiments may represent a small population of proliferating cells at different stages of their cell cycles.

Given that the contraction frequency was decreased by the T-type Ca^{2+} channel inhibitor, we can conclude that this channel contributes to uterine autorhythmicity alongside other inward conductances.

In conclusion, we found no evidence for slow-propagating intercellular $[Ca^{2+}]_i$ waves mediating gradual recruitment of myocytes within myometrial bundles. Our data suggest that the spread of $[Ca^{2+}]_i$ signals in human myometrium is achieved *via* propagation of long-lasting action potentials. This spread is fast when action potentials propagate along the bundles of myocytes and slows down during propagation between the bundles. The role of myometrial telocytes and fibroblasts in uterine E-C coupling remains unclear and warrants further investigation.

Acknowledgements

This work was supported by a project grant from the BBSRC, UK (BB/D016630/1 to A. Shmygol) and by the Reproductive Health Biomedical Research Unit, University Hospital Coventry and Warwickshire.

Conflict of interest

The authors confirm that there are no conflicts of interest.

References

1. **Bolton TB.** Cholinergic Mechanisms in Smooth-Muscle. *Br Med Bull*. 1979; 35: 275–83.
2. **Kuriyama H, Kitamura K, Itoh T, *et al.*** Physiological features of visceral smooth muscle cells, with special reference to receptors and ion channels. *Physiol Rev*. 1998; 78: 811–920.
3. **Wikland M, Lindblom B.** Relationship between electrical and mechanical activity of the isolated term-pregnant human myometrium. *Eur J Obstet Gynecol Reprod Biol*. 1985; 20: 337–46.
4. **Nakao K, Inoue Y, Okabe K, *et al.*** Oxytocin enhances action potentials in pregnant human myometrium - A study with microelectrodes. *Am J Obstet Gynecol*. 1997; 177: 222–8.
5. **Kawarabayashi T, Izumi H, Ikeda M, *et al.*** Modification by Magnesium of the Excitatory Effect of Oxytocin in Electrical and Mechanical Activities of Pregnant Human Myometrium. *Obst Gynecol*. 1990; 76: 183–8.
6. **Parkington HC, Tonta MA, Brennecke SP, *et al.*** Contractile activity, membrane potential, and cytoplasmic calcium in human uterine smooth muscle in the third trimester of pregnancy and during labor. *Am J Obst Gynecol*. 1999; 181: 1445–51.
7. **Garfield RE, Sims S, Daniel EE.** Gap Junctions - Their Presence and Necessity in Myometrium during Parturition. *Science*. 1977; 198: 958–60.
8. **Miyoshi H, Boyle MB, MacKay LB, *et al.*** Gap junction currents in cultured muscle cells from human myometrium. *Am J Obst Gynecol*. 1998; 178: 588–93.
9. **Sakai N, Tabb T, Garfield RE.** Modulation of Cell-to-Cell Coupling between Myometrial Cells of the Human Uterus during Pregnancy. *Am J Obst Gynecol*. 1992; 167: 472–80.
10. **Garfield RE, Hayashi RH, Harper MJK.** Invitro Studies on the Control of Human Myometrial Gap-Junctions. *Int J Gynecol Obstet*. 1987; 25: 241–8.
11. **Shmygol A, Blanks AM, Bru-Mercier G, *et al.*** Tissue-level Ca^{2+} signalling in human myometrium: a possible role for ICCs. *Proc Physiol Soc*. 2006; 3: 75–76.
12. **Ciontea SM, Radu E, Regalia T, *et al.*** C-kit immunopositive interstitial cells (Cajal-type) in human myometrium. *J Cell Mol Med*. 2005; 9: 407–20.
13. **Duquette RA, Shmygol A, Vaillant C, *et al.*** Vimentin-positive, c-KIT-negative interstitial cells in human and rat uterus: A role in pacemaking? *Biol Reprod*. 2005; 72: 276–83.
14. **Popescu LM, Faussone-Pellegrini MS.** TELOCYTES - a case of serendipity: the winding way from Interstitial Cells of Cajal (ICC), *via* Interstitial Cajal-Like Cells (ICLC) to TELOCYTES. *J Cell Mol Med*. 2010; 14: 729–40.
15. **Popescu LM, Vidulescu C, Curici A, *et al.*** Imatinib inhibits spontaneous rhythmic contractions of human uterus and intestine. *Eur J Pharmacol*. 2006; 546: 177–81.

16. **Young RC.** Myocytes, myometrium, and uterine contractions. *Ann N Y Acad Sci*. 2007; 1101: 72–84.
17. **Young RC, Hession RO.** Three-dimensional structure of the smooth muscle in the term-pregnant human uterus. *Obst Gynecol*. 1999; 93: 94–9.
18. **McKillen K, Thornton S, Taylor CW.** Oxytocin increases the $[Ca^{2+}](i)$ sensitivity of human myometrium during the falling phase of phasic contractions. *Am J Physiol*. 1999; 276: E345–51.
19. **Word RA, Tang DC, Kamm KE.** Activation Properties of Myosin Light-Chain Kinase during Contraction-Relaxation Cycles of Tonic and Phasic Smooth Muscles. *J Biol Chem*. 1994; 269: 21596–602.
20. **Fomin VP, Gibbs SG, Vanam R, *et al.*** Effect of magnesium sulfate on contractile force and intracellular calcium concentration in pregnant human myometrium. *Am J Obstet Gynecol*. 2006; 194: 1384–90.
21. **Fomin VP, Kronbergs A, Gunst S, *et al.*** Role of Protein Kinase C alpha in Regulation of [Ca(2+)](I) and Force in Human Myometrium. *Reprod Sci*. 2009; 16: 71–9.
22. **Longbottom ER, Luckas MJM, Kupittayanant S, *et al.*** The effects of inhibiting myosin light chain kinase on contraction and calcium signalling in human and rat myometrium. *Pflugers Arch*. 2000; 440: 315–21.
23. **Luckas M, Longbottom T, Shmigol T, *et al.*** Calcium-independent force production by human myometrium? *Br J Obstet Gynaecol*. 2000; 107: 815–6.
24. **Young RC, Hession RO.** Intra- and intercellular calcium waves in cultured human myometrium. *J Muscle Res Cell Motil*. 1996; 17: 349–55.
25. **Shlykov SG, Sanborn BA.** Stimulation of intracellular Ca^{2+} oscillations by diacylglycerol in human myometrial cells. *Cell Calcium*. 2004; 36: 157–64.
26. **Burdyga T, Borisova L, Burdyga AT, *et al.*** Temporal and spatial variations in spontaneous Ca events and mechanical activity in pregnant rat myometrium. *Eur J Obstet Gynecol Reprod Biol*. 2009; 1445: s25–32.
27. **Maravall M, Mainen ZF, Sabatini BL, *et al.*** Estimating intracellular calcium concentrations and buffering without wavelength ratioing. *Biophys J*. 2000; 78: 2655–67.
28. **Blanks AM, Zhao ZH, Shmygol A, *et al.*** Characterization of the molecular and electrophysiological properties of the T-type calcium channel in human myometrium. *J Physiol (Lond)*. 2007; 581: 915–26.
29. **Young RC.** Tissue-level signaling and control of uterine contractility: the action potential-calcium wave hypothesis. *J Soc Gynecol Investig*. 2000; 7: 146–52.
30. **Bui PH, Quesada A, Handforth A, *et al.*** The mibefradil derivative NNC55-0396, a specific T-type calcium channel antagonist, exhibits less CYP3A4 inhibition than mibefradil. *Drug Metab Dispos*. 2008; 36: 1291–9.
31. **Huang LP, Keyser BM, Tagmose TM, *et al.*** NNC 55-0396 [(1S, 2S)-2-(2-(N-[(3-benzimidazol-2-yl) propyl]-N-methylamino)ethyl)-6-fluoro-1,2,3,4-tetrahydro-1-isopropyl-2-naphtyl cyclopropanecarboxylate dihydrochloride]: a new selective inhibitor of T-type calcium channels. *J Pharmacol Exp Ther*. 2004; 309: 193–9.
32. **Vauge C, Carbonne B, Papiernik E, *et al.*** A mathematical model of uterine dynamics and its application to human parturition. *Acta Biotheor*. 2000; 48: 95–105.
33. **Young RC.** A computer model of uterine contractions based on action potential propagation and intercellular calcium waves. *Obst Gynecol*. 1997; 89: 604–8.
34. **Ohkubo T, Inoue Y, Kawarabayashi T, *et al.*** Identification and electrophysiological characteristics of isoforms of T-type calcium channel Ca(v)3.2 expressed in pregnant human uterus. *Cell Physiol Biochem*. 2005; 16: 245–54.
35. **Rodman DM, Reese K, Harral J, *et al.*** Low-voltage-activated (T-type) calcium channels control proliferation of human pulmonary artery myocytes. *Circ Res*. 2005; 96: 864–72.
36. **Sui GP, Wu C, Fry CH.** A description of Ca(2+) channels in human detrusor smooth muscle. *Bju Int*. 2003; 92: 476–82.
37. **Lee SE, Ahn DS, Lee YH.** Role of T-type Ca (2+) Channels in the Spontaneous Phasic Contraction of Pregnant Rat Uterine Smooth Muscle. *Korean J Physiol Pha*. 2009; 13: 241–9.